Cyclic Peptide Analysis of the Biologically Active Loop Region in the Laminin α3 Chain LG4 Module Demonstrates the Importance of Peptide Conformation on Biological Activity†

Kozue Kato-Takagaki,‡,§ Nobuharu Suzuki,§ Fumiharu Yokoyama,§ Shu Takaki,‡ Koji Umezawa,|| Junichi Higo,|| Mayumi Mochizuki,§ Yamato Kikkawa,‡ Shinya Oishi,⊥ Atsushi Utani,# and Motoyoshi Nomizu*,‡

Laboratory of Clinical Biochemistry, School of Pharmacy, and Laboratory of Bioinformatics, School of Life Science, Tokyo University of Pharmacy and Life Sciences, Hachioji, Tokyo 192-0392, Division of Bioscience, Graduate School of Environmental Earth Science, Hokkaido University, Sapporo 060-0810, Graduate School of Pharmaceutical Sciences, Kyoto University, Kyoto 606-8501, and Department of Dermatology, Graduate School of Medicine, Kyoto University, Kyoto 606-8507, Japan

Received October 9, 2006; Revised Manuscript Received December 2, 2006

ABSTRACT: The laminin α3 chain LG4 module (α3LG4 module) has cell adhesion, heparin binding, migration, and neurite outgrowth activities. The LG4 module consists of a 14-stranded *β*-sheet (A-N) sandwich structure. Previously, we identified the A3G756 sequence (KNSFMALYLSKGRLVFALG in the human laminin α3 chain 1411−1429) as a biologically active site in the α3LG4 module. The A3G756 sequence is located on the E and F strands based on a crystal structure-based sequence alignment. The Lys^{1421} and Arg^{1423} residues, critical amino acids for the biological activity of A3G756, are located on the E−F connecting loop region as a KGR sequence. In this study, we focused on the KGR sequence and investigated the structural requirements of the E−F connecting loop region in the α3LG4 module. We synthesized three linear peptides containing the KGR sequence at the middle and the N and C termini and also prepared three cyclic analogues corresponding to the linear peptides. *cyclo*-hEF3A (CLYLSKGR-LVFAC), which is a cyclic peptide containing the KGR sequence at the middle, showed the strongest inhibitory effect on both the heparin binding and the cell attachment to the recombinant α3LG4 module protein. The *cyclo*-hEF3A peptide was more active for syndecan-4 binding and neurite outgrowth than the linear form. Furthermore, we found that the structure of *cyclo*-hEF3A is similar to that of the connecting E−F loop region in human laminin α3LG4 module by structural analysis using molecular dynamics simulations. These results suggest that the loop structure of the E−F connecting region of the α3LG4 module is important for its biological activities. The *cyclo*-hEF3A peptide may be useful for the development of therapeutic reagents especially for wound healing and nerve regeneration.

Laminins, a multifunctional glycoprotein in basement membranes, are expressed in a tissue-specific manner and have diverse biological functions, including promotion of cell adhesion, migration, proliferation, differentiation, neurite outgrowth, angiogenesis, and tumor metastasis (*1*, *2*). Laminins are heterotrimeric proteins consisting of three distinct α-, *β*-, and *γ*-chains. So far, five α-, three *β*-, and three *γ*-chains have been identified (*3*, *4*). At least 15 isoforms (laminin-1−15) are formed by various combinations of each subunit (*3*−*5*). Laminin-5 (α3, *β*3, *γ*2) is mainly expressed in the skin and promotes keratinocyte adhesion (*6*). Laminin-5 is also expressed in the floor plate of the developing neural tube (*7*) and has been shown to promote neurite outgrowth (*8*−*10*). The laminin α3 chain, a subunit of laminin-5, contains a unique C-terminal globular domain (G domain). The G domain consists of five tandem laminin G-like modules (LG1−5) and plays important roles in laminin α3 chain−cell interactions.

Previously, we demonstrated that the LG4 module was the major active module for cell adhesion, heparin binding, migration, and neurite outgrowth in the laminin α3 chain G domain (*11*−*13*). We identified the A3G756 sequence (KNSFMALYLSKGRLVFALG, human laminin α3 chain 1411−1429) as a biologically active site in the α3LG4 module (*11*−*13*). Using mutagenesis analysis of recombinant α3LG4 protein, we also found that the two basic residues, Lys^{1421} and Arg^{1423}, in the A3G756 sequence were critical for the biological activity (*11*).

The crystal structure of mouse laminin α2 chain LG5 module revealed that it forms a 14-stranded *β*-sheet (A−N strands) sandwich structure (*14*). The A3G756 sequence is located on the E and F strands based on a structure-based sequence alignment (*11*, *15*). The Lys^{1421} and Arg^{1423}

† This work was supported by Grants-in-Aid for Scientific Research from the Ministry of Education, Cultures, Sports, Science and Technology of Japan (17390024, 17014081, and 18060041).

* To whom correspondence should be addressed. Tel/Fax: 81-426-76-5662. E-mail: nomizu@ps.toyaku.ac.jp.

‡ School of Pharmacy, Tokyo University of Pharmacy and Life Sciences.

§ Hokkaido University.

|| School of Life Science, Tokyo University of Pharmacy and Life Sciences.

⊥ Graduate School of Pharmaceutical Sciences, Kyoto University.

Graduate School of Medicine, Kyoto University.

10.1021/bi062098l CCC: $37.00
Published on Web 01/30/2007

residues, the critical amino acids for the biological activity of A3G756, are located on the E−F connecting loop region as a KGR sequence. Additional studies also suggested that the E−F loop region of the LG4 module plays an important role for the biological activity of the laminin α1 and α4 chains (*16*−*18*). Recently, the A3G756 peptide has been found to promote wound healing in vivo (Momota et al., unpublished results). Thus, the A3G756 peptide has potential as a therapeutic reagent.

Arg-Gly-Asp (RGD) and Tyr-Ile-Gly-Ser-Arg (YIGSR) sequences are located in a loop region of the fibronectin tenth type III module and in the laminin β1 chain domain III, respectively (*19*, *20*). A loop structure of the RGD and YIGSR peptides is suggested to be important for biological activity (*21*, *22*). Cyclization of the peptide leads to formation of the loop structure and enhances the biological activity. For example, cyclic RGD peptides blocked cell adhesion to a fibronectin substrate better than the linear peptide (*21*). A cyclic YIGSR peptide enhanced cell attachment activity and increased inhibition of tumor metastasis better than the linear form (*23*). These observations indicate that a cyclic peptide approach may be useful to investigate the structural significance of a loop structure in proteins. Furthermore, the cyclic peptide approach may be useful for drug development of peptides (*24*).

In this study, we focus on the structural significance of the connecting loop region of the E and F strands in the laminin α3 chain LG4 module. To demonstrate the structural requirement of the E−F loop region, we synthesized various linear and cyclic peptides that contained a KGR sequence and tested their biological activities. We found that a cyclic peptide, *cyclo*-hEF3A (CLYLSKGRLVFAC), strongly inhibited heparin binding and cell attachment to the recombinant α3LG4 protein.

MATERIALS AND METHODS

Cells and Culture. Human neonatal dermal fibroblasts (IWAKI Co. Ltd., Tokyo, Japan), HaCat human keratinocyte cells, and 293T human renal epithelial cells (*25*) were cultured in Dulbecco's modified Eagle's medium (DMEM; Invitrogen, Carlsbad, CA) containing 10% fetal bovine serum (FBS; Invitrogen), 100 units/mL penicillin, and 100 μg/mL streptomycin (Invitrogen). PC12 rat pheochromocytoma cells (*26*) were cultured in DMEM containing 7.5% horse serum (Invitrogen), 7.5% FBS, 100 units/mL penicillin, and 100 μg/mL streptomycin. The cells were maintained at 37 °C in a humidified 5% CO_2/95% air atmosphere.

Recombinant Protein. Recombinant laminin α3 LG4 protein (rec-α3LG4) was expressed as a chimera with a human IgG Fc portion at the C terminus and purified as previously described with a minor modification (*11*). The plasmid was transfected into 293T cells using the FuGENE6 transfection reagent (Roche Diagnostics, Basel, Switzerland). Conditioned medium (CM) with 1.5% FBS in DMEM was collected for 5 days at 24 h intervals, and 1 mM PMSF (Sigma, St. Louis, MO) was added. CM was applied to a protein A-affinity column (HiTrap Protein A HP; GE Healthcare Bio-Sciences Corp., Piscataway, NJ) equilibrated in buffer A [10 mM Tris-HCl (pH 7.4) containing 150 mM NaCl, 2 mM EDTA, and 0.5 mM N-ethylmaleimide]. The bound protein was eluted with 0.1 M glycine-HCl (pH 2.7) and immediately neutralized by 1 M Tris-HCl (pH 8.8). The eluted sample was applied to a heparin affinity column (HiTrap Heparin HP; GE Healthcare Bio-Sciences Corp.) equilibrated in buffer A. The bound protein was eluted with buffer A in the presence of 1 M NaCl. The rec-α3LG4 protein was detected with biotinylated anti-human IgG (Jackson ImmunoResearch Laboratories, West Grove, PA) and streptavidin-peroxidase (Sigma) in Western blotting. The protein concentration was determined by BCA assay kit (Pierce, Rockford, IL) with bovine serum albumin (BSA; Sigma) as the standard.

Synthetic Peptides. All linear peptides were manually synthesized by the 9-fluorenylmethoxycarbonyl (Fmoc)-based solid-phase method with a C-terminal amide as described previously (*27*). The respective amino acids were condensed manually in a stepwise manner using diisopropylcarbodiimide-*N*-hydroxybenzotriazole on a Rink amide resin (Merck KGaA, Darmstadt, Germany). The side chain protecting groups were used as follows: Asn and Cys, trityl; Asp, Ser, Thr, and Tyr, *t*-butyl; Arg, 2,2,4,6,7-pentamethyldihydrobenzofuran-5-sulfonyl; and Lys, *t*-butoxycarbonyl. The resulting protected peptide resins were deprotected and cleaved from the resin using trifluoroacetic acid/thioanisole/*m*-cresol/ethanedithiol/H_2O (80:5:5:5:5, v/v) at 20 °C for 3 h. Crude peptides were precipitated and washed with ethyl ether and then purified by reverse-phase high-performance liquid chromatography (HPLC) (using a Vydac 5C18 column with a gradient of H_2O/acetonitrile containing 0.1% trifluoroacetic acid).

Cyclic peptides were synthesized using a similar protocol to that described above with some modifications. Methionine residue was replaced with norleucine, since the amino acid may be oxidized during the cyclization step. Protected peptide resins were prepared on a NovaSyn TGR resin (Merck KGaA) by the Fmoc-based solid-phase synthesis. Treatment of the protected peptide resin with a solution of trifluoroacetic acid/1,2-ethanedithiol/H_2O (95:2.5:2.5, v/v) at 20 °C for 3 h afforded a linear peptide, which was precipitated with ethyl ether. The linear peptides were cyclized by oxidation in a mixture of H_2O/acetic acid/dimethyl sulfoxide (45:45:10, v/v/v) at room temperature for 2 days and purified by reverse-phase HPLC using a Cosmosil 5C18-ARII column (Nacalai Tesque, Kyoto, Japan) with a gradient of water/acetonitrile containing 0.1% trifluoroacetic acid. The purity and identity of the synthetic peptides were confirmed by LC-MS.

Inhibition of Heparin Binding to rec-α3LG4. The effect of peptides on heparin binding to rec-α3LG4 was tested using heparin-Sepharose beads as previously described with some modifications (*18*). The rec-α3LG4 protein (0.7 μg) was incubated with heparin-Sepharose beads (1 mg, GE Healthcare Bio-Sciences Corp.) in 70 μL of buffer B [10 mM Tris-HCl (pH 7.4) containing 100 mM NaCl] in the presence of various concentrations of peptides at 4 °C for 1 h, and then, the beads were collected by centrifugation. The supernate was removed, and the beads were washed twice with buffer B. The rec-α3LG4 protein bound to the beads was extracted with sodium dodecyl sulfate−polyacrylamide gel electrophoresis (SDS-PAGE) sample buffer (15 μL) and analyzed by SDS-PAGE in 10% acrylamide gels under reducing conditions. The rec-α3LG4 protein was detected by Western blotting using biotinylated anti-human IgG and streptavidin-

conjugated horseradish peroxidase. The intensity of the bands was quantified by ImageJ 1.36 software.

Cell Attachment Assay. The cell attachment assay using rec-α3LG4 and synthetic peptides was performed in 96 well plates (DYNEX Technologies, Chantilly, VA). The rec-α3LG4 protein (0.002−2 μg) in buffer A (50 μL) was added to 96 wells and incubated overnight at 4 °C. Synthetic peptides were dissolved in Milli-Q water (0.0001−0.4 mg/mL), and the solution (50 μL) was added to each well, followed by drying overnight at room temperature. After coating protein or peptides, the plates were blocked with 1% heat-denatured BSA in DMEM at 37 °C for 1 h and then washed with 0.1% BSA in DMEM. Fibroblast and HaCat cells were detached with 0.02% trypsin-EDTA (Invitrogen). PC12 cells were harvested by agitation. The cells were allowed to recover in their respective culture medium for 20 min at 37 °C. After they were washed two times with 0.1% BSA in DMEM, cells were resuspended in 0.1% BSA in DMEM, plated at 2.0×10^4 cells/100 μL/well, and incubated at 37 °C for 1 h in 5% CO_2. The medium was removed by aspiration, and the attached cells were stained with 0.2% crystal violet aqueous solution in 20% methanol for 10 min. After the wells were washed with water, 1% SDS solution (150 μL) was added to each well to dissolve the cells. The optical density at 570 nm was measured in a model 550 microplate reader (Bio-Rad Laboratories, Hercules, CA).

In peptide inhibition experiments, 96 well plates were coated with rec-α3LG4 as described above. Cells were preincubated with various concentrations of peptide in 0.1% BSA in DMEM at 37 °C for 10 min, and then, cells (2.0×10^4 cells/100 μL/well) were added to the plates and incubated at 37 °C for 30 min in 5% CO_2. The attached cells were quantified as described above.

In heparin and EDTA inhibition experiments, 96 well plates were coated with peptide as described above. Fibroblasts were preincubated for 10 min at 37 °C with heparin (10 μg/mL) or EDTA (5 mM) prior to plating in the wells. After the cells (2.0×10^4 cells/100 μL/well) were incubated at 37 °C for 30 min in 5% CO_2, the attached cells were measured as described above.

Solid-Phase Syndecan-4 Binding Assay. Syndecan-4 binding to peptide-coated plates was examined using a human neonatal dermal fibroblast lysate. The fibroblast lysate was prepared as described previously (*11*). Various amounts of peptides in Milli-Q water (50 μL) were coated onto 96 well plates (Nalge Nunc International, Rochester, NY) and dried overnight at room temperature. The wells were blocked with 20% BlockAce (Dainippon Sumitomo Pharma Co., Osaka, Japan) and 0.05% Tween 20 in PBS at room temperature for 30 min. The fibroblast lysate was diluted to 10% (v/v) with buffer C (10% Block Ace and 0.05% Tween 20 in PBS). The fibroblast lysate solution (50 μL/well) was added to each well and incubated at 37 °C for 1 h. In the heparin inhibition experiments, the fibroblast lysate was incubated with 25 μg/well of heparin. After the wells were washed with buffer D (0.05% Tween 20 in PBS), anti-syndecan-4 monoclonal antibody (5G9; Santa Cruz Biotechnology, Santa Cruz, CA) in buffer C (1:1000, v/v) was added and incubated at 37 °C for 30 min. The wells were washed with buffer D, and then, biotinylated anti-mouse IgG antibody (Vector Laboratories, Burlingame, CA) in buffer C (1:2500, v/v) was added and incubated at 37 °C for 30 min. After the wells were washed with buffer D, streptavidin-conjugated horseradish peroxidase in buffer C (1:2500, v/v) was added and incubated at 37 °C for 30 min. After they were washed with buffer D, 3,3′,5,5′-tetramethyl-benzidine (TMB) solution (50 μL/well, Sigma) was added to the wells and incubated at room temperature for 30 min. After addition of 0.5 M H_2SO_4 (50 μL/well, Wako), the optical density at 450 nm was measured using a model 550 microplate reader.

Neurite Outgrowth Assay. Neurite outgrowth was performed in 96 well plates (DYNEX) coated with peptides as described above. After the peptides were coated, the plates were washed with DMEM/F12 (Invitrogen). PC12 cells were primed with 100 ng/mL of nerve growth factor (NGF, Roche Diagnostics) for 24 h prior to the assay. The PC12 cells were then collected by agitation, allowed to recover in the cultured medium for 30 min at 37 °C in 5% CO_2, and washed two times with DMEM/F12. After they were washed, cells were resuspended in DMEM/F12 containing 100 μg/mL transferrin (Sigma), 20 nM progesterone (Sigma), 30 nM Na_2SeO_3 (Wako, Osaka, Japan), 5 μg/mL insulin (Invitrogen), and 100 ng/mL NGF. The cells were added to 96 well plates at 3.0×10^3 cells/100 μL/well. After incubation at 37 °C for 24 h in 5% CO_2, the cells were fixed with 20% formalin and then stained with crystal violet. In each well, 100 cells were viewed and the percent of the active cells, which had neurites that extended two times the cell diameter in length or longer, was determined.

Structural Analysis. The human laminin α3LG4 module is homologous to the laminin α2LG4 module. The crystal structure of the laminin α2 chain, which involves the LG4 and LG5 modules, was published (PDB ID: 1DYK). We determined the region corresponding to hEF3A in laminin α2LG4 module by sequence alignment and refer to this region as homologous_hEF3A.

We prepared two peptides, 1DYK_SS and *cyclo*-hEF3A. 1DYK_SS has the same sequence as homologous_hEF3A except for the N and C termini, which are replaced by Cys residues with a disulfide bond between them. The simulation of 1DYK_SS was performed to measure the effect of the disulfide bond on the conformation. The structure of homologous_hEF3A was used as the template for starting the simulations of 1DYK_SS and *cyclo*-hEF3A.

We carried out the simulations with the AMBER C96 (*28*) and generalized Born/surface area (GBSA) methods (*29*). The energy of each peptide was minimized by a steepest descent method. For obtaining the native states of peptide, we implemented simulated annealing molecular dynamics (MD) simulations with the SHAKE algorithm (*30*). The Hoover−Evans Gaussian constraint method (*31*) was employed to control the temperature. The computer program used was PRESTO X v2.1 (*32*−*34*). The time step was 2.0 fs/step. The whole computational process was performed in three successive stages: heating, high-temperature (1000 K) sampling, and annealing. At the heating, the temperature was increased from 0 to 1000 K for 2.0 ns. At the sampling, we stored a structure every 10 ps from the simulation for 2.0 ns. Thus, a total of 100 structures for each of peptide were stored at 1000 K. Because the temperature of 1000 K was high enough to unfold initial conformation of the peptide, the obtained 100 conformations distributed with a large variety. In the annealing, each stored structure was annealed

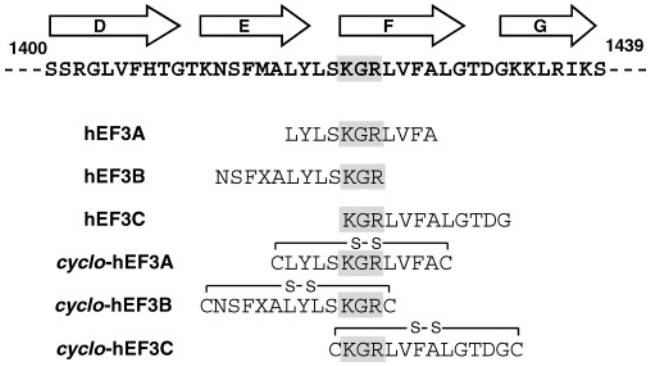

FIGURE 1: Linear and cyclic peptides from the laminin α3 chain LG4 module. The sequence of the LG4 module is shown at the top (*49*). The arrows represent *β*-strands (*14*, *15*). The shaded area denotes the KGR sequence. The single letter X denotes norleucine residue. All peptides have C-terminal amides.

from 1000 to 300 K, taking 1.0 ns for each run. Finally, we obtained 100 structures at 300 K for each of the peptides.

The root-mean-square deviation (RMSD) was calculated for the main chain atoms (Cα, C, and N) of residues 3−11 between structures sampled from the structure of homologous_hEF3A and MD simulation. The structures obtained from the MD simulation were classified into three clusters by the RMSD value for each of the peptides.

RESULTS

Design of Cyclic Peptides from the Laminin α3 Chain LG4 Module. Previously, we showed that the laminin α3 chain LG4 module has a heparin binding activity and promotes cell attachment, migration, and neurite outgrowth using a recombinant human laminin α3 chain LG4 protein (rec-α3LG4) (*11*−*13*). We also showed that the KGR sequence in the loop region between the E and the F strands was critical for the biological activity (*11*). Here, we focused on the KGR sequence and the structural requirements of the loop region. We designed and prepared three linear peptides containing the KGR sequence at the middle and the N and C termini (Figure 1). We also prepared three cyclic analogues corresponding to the linear peptides (Figure 1). We evaluated the conformational effect of the loop region on the biological activity using the linear and cyclic peptides.

Effect of Peptides on the Heparin Binding of rec-α3LG4. We first examined the inhibitory effect of the linear peptides on heparin binding to the rec-α3LG4 protein. All of the linear peptides showed an inhibitory effect (Figure 2). The hEF3B peptide strongly inhibited (Figure 2B) while hEF3A and hEF3C showed weaker activity (Figure 2A,C). This result indicates that the KGR sequence on the flexible C terminus in the peptide is preferable for the heparin binding.

Next, we examined the inhibitory effect of the cyclic peptides relative to the linear forms. Two cyclic peptides, *cyclo*-hEF3A and *cyclo*-hEF3C, showed an increased inhibitory effect on heparin binding of rec-α3LG4 relative to the linear forms (Figure 2A,C). In contrast, the *cyclo*-hEF3B showed a weaker inhibitory effect as compared with that of the linear peptide (Figure 2B). The *cyclo*-hEF3A showed the strongest inhibitory effect of the synthetic peptides. The data suggest that the loop structure of the hEF3A sequence is important for the heparin binding.

Effect of Peptides on Cell Attachment to rec-α3LG4. Next, the inhibitory effect of the six peptides on fibroblast attachment to the rec-α3LG4 protein was examined (Figure 3A). Fibroblast attached to the rec-α3LG4 protein in a dose-dependent manner (data not shown). *cyclo*-hEF3A strongly inhibited fibroblast attachment to rec-α3LG4 relative to that of the linear peptide hEF3A (Figure 3A). The inhibitory effect of *cyclo*-hEF3B was comparable to that of the linear peptide hEF3B (Figure 3A). hEF3C slightly inhibited, but *cyclo*-hEF3C did not affect fibroblast attachment to rec-α3LG4 (Figure 3A). These results suggest that the peptide conformation is important for fibroblast attachment to rec-α3LG4. The *cyclo*-hEF3A peptide had the strongest inhibitory effect on both heparin binding and fibroblast attachment to rec-α3LG4 (Figures 2 and 3A). Therefore, we focused on the hEF3A and *cyclo*-hEF3A peptides and further examined the conformational requirements for biological activity.

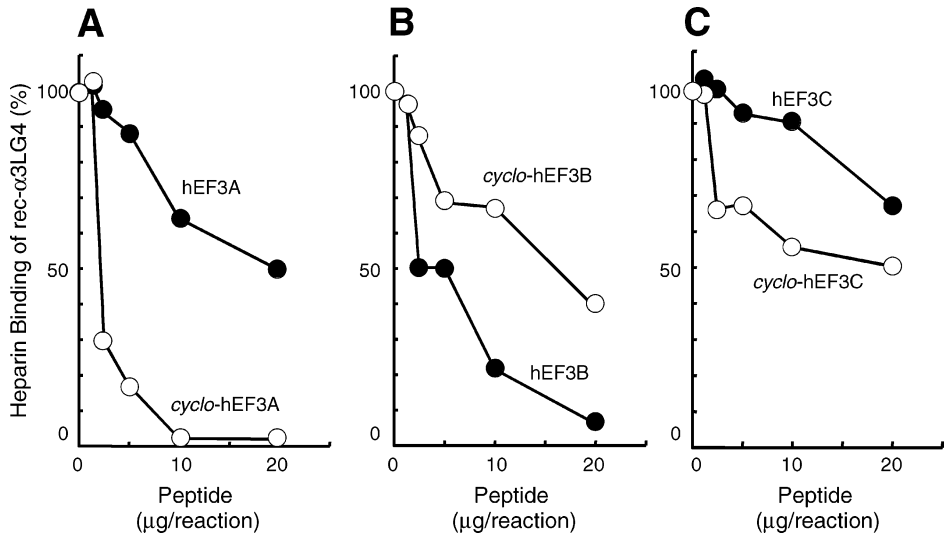

FIGURE 2: Effect of peptides on heparin binding to rec-α3LG4. Heparin-Sepharose beads (1 mg) with various amounts of peptide and rec-α3LG4 (0.7 *μ*g) were incubated in 70 *μ*L of 10 mM Tris buffer (pH 7.4) containing 100 mM NaCl at 4 °C for 1 h. After the beads were washed with the buffer, the rec-α3LG4 bound to the heparin-Sepharose beads was detected with biotinylated anti-human IgG and streptavidin-peroxidase in Western blotting. The intensity of the bands was quantified using ImageJ 1.36 software. Triplicate experiments gave similar results.

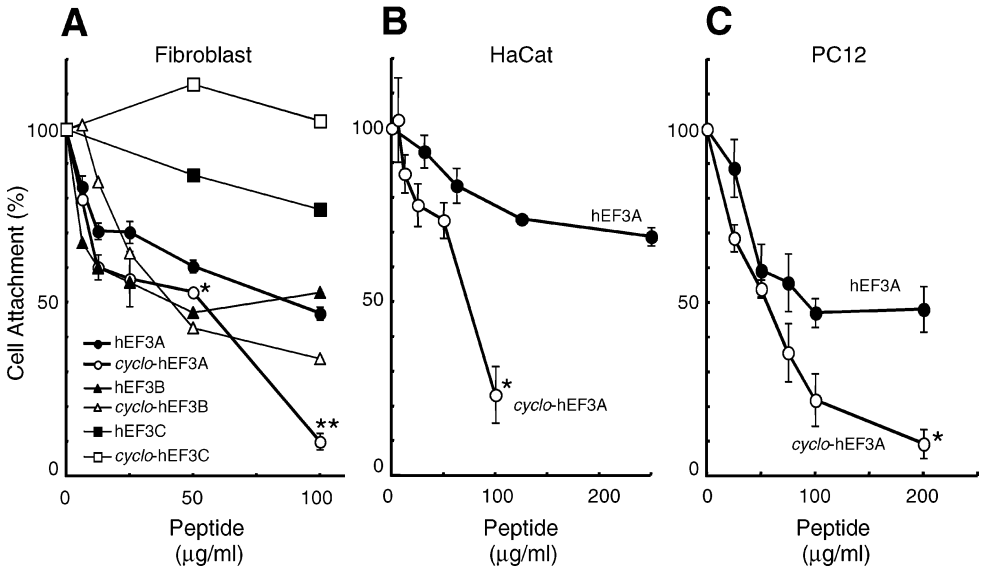

FIGURE 3: Effect of peptides on cell attachment to rec-α3LG4 using fibroblasts (A), HaCat cells (B), and PC12 cells (C). Plates (96 well) were coated with rec-α3LG4 (0.7 μg/well for fibroblasts and HaCat cells; 1 μg/well for PC12 cells). Cells (2.0×10^4 cells/well) were preincubated with various concentrations of peptides for 10 min and added to the rec-α3LG4-coated plates. After a 30 min incubation, the number of attached cells was assessed by staining with crystal violet. Data of hEF3A and *cyclo*-hEF3A are expressed as means ± SE of triplicate experiments. *, $p < 0.05$; **, $p < 0.01$.

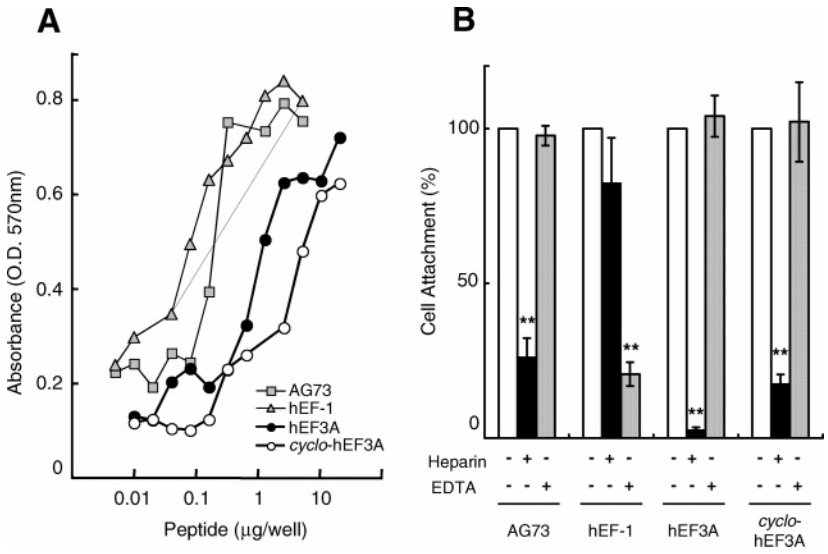

FIGURE 4: Fibroblast attachment to peptides (A) and effect of heparin and EDTA on the cell attachment (B). (A) Various amounts of peptides were coated on 96 well plates, and fibroblasts (2.0×10^4 cells/well) were added to the wells. After a 1 h incubation, the number of attached cells was assessed by staining with crystal violet. (B) Plates (96 well) were coated with AG73 (0.5 μg/well), hEF-1 (1.5 μg/well), hEF3A (10 μg/well), and *cyclo*-hEF3A (10 μg/well). AG73 (RKRLQVQLSIRT, mouse laminin α1 chain 2719−2730) (*35*) and hEF-1 (DYAVLQLHGGRLHFMFDLG, human α1 chain 2762−2780) (*36*) were used as positive controls for heparin and EDTA, respectively. Fibroblasts (2.0×10^4 cells/well) were preincubated with either heparin (10 μg/mL) or EDTA (5 mM) for 10 min and added to the peptide-coated plates. After a 30 min incubation, attached cells were assessed by staining with crystal violet. The fibroblast attachment activity in the absence of heparin and EDTA was taken as 100%. Data are expressed as means ± SD of triplicate results. Duplicate experiments gave similar results. **, $p < 0.01$.

Next, we tested the inhibitory effect of hEF3A and *cyclo*-hEF3A on the cell attachment to rec-α3LG4 using human keratinocyte HaCat cells (Figure 3B) and rat pheochromocytoma PC12 cells (Figure 3C). Both cells attached to the rec-α3LG4 protein in a dose-dependent manner (data not shown). *cyclo*-hEF3A showed a stronger inhibitory effect on the attachment of both cell types to the protein than that of the linear peptide hEF3A (Figure 3B,C). These results also suggested that the loop conformation is important for cell attachment activity of the hEF3A sequence.

Cell Attachment Activity of Peptides. We evaluated the cell attachment activity of hEF3A and *cyclo*-hEF3A using fibroblasts. We used AG73 (RKRLQVQLSIRT, mouse laminin α1 chain residues 2719−2730) and hEF-1 (DYAVLQLHGGRLHFMFDLG, human α1 chain residues 2762−2780) as controls for heparin- and cation-dependent cell attachment, respectively. AG73 promotes a syndecan-mediated cell attachment (*35*), and hEF-1 promotes an α2β1 integrin-mediated cell attachment (*36*). The AG73 and hEF-1 peptides showed cell attachment activity as expected (Figure 4A). *cyclo*-hEF3A promoted cell attachment activity in a dose-dependent manner similar to that of hEF3A (Figure 4A). We also tested the effects of heparin and EDTA on cell attachment to the peptides. As described previously, cell

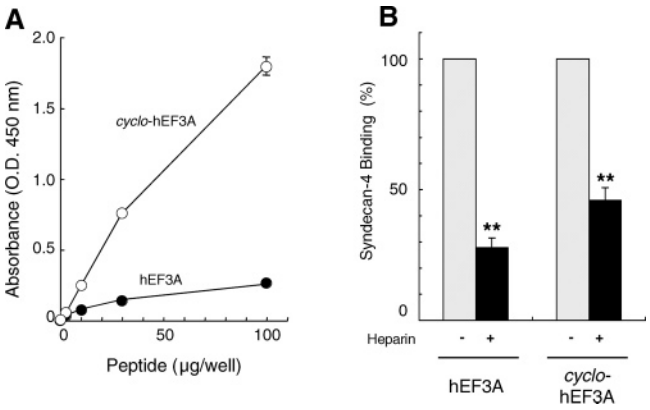

FIGURE 5: Syndecan-4 binding to peptides (A) and effect of heparin on the syndecan-4 binding (B). (A) Various amounts of peptides were coated on 96 well plates. Fibroblast lysate was added to the 96 well plate and incubated at 37 °C for 1 h. Syndecan-4 bound to the peptide-coated plates was quantitated by anti-syndecan-4 antibody, biotinylated anti-mouse IgG antibody, and streptavidin-conjugated horseradish peroxidase. Data are expressed as means ± SD of duplicate results. Triplicate experiments gave similar results. (B) Plates (96 well) were coated with hEF3A and *cyclo*-hEF3A (30 μg/well). Fibroblast lysate and heparin (25 μg/well) were added to the peptide-coated plates. After a 1 h incubation, syndecan-4 bound to the peptide-coated plates was quantitated as described above. Syndecan-4 binding in the absence of heparin was taken as 100%. Data are expressed as means ± SD of duplicate results. Triplicate experiments gave similar results. **, $p < 0.01$.

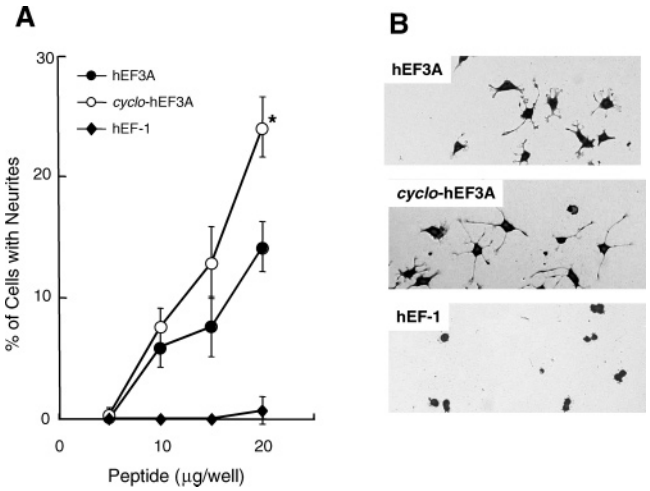

FIGURE 6: Neurite outgrowth of PC12 cells on peptides. (A) Various amounts of peptides were coated on 96 well plates. PC12 cells (3.0×10^3 cells/well) were seeded in the plates and incubated for 24 h. After cells were fixed and stained, the percentage of cells with neurites was determined as described under the Materials and Methods. Data are expressed as means ± SD of triplicate results. Triplicate experiments gave similar results. *, $p < 0.05$. (B) Photographs of the PC12 cells cultured on 20 μg/well of hEF3A, *cyclo*-hEF3A, and hEF-1 for 24 h. Cells were fixed and stained and then photographed with a 200× objective on a microscope.

attachment on AG73 and hEF-1 was inhibited by heparin and by EDTA, respectively (*35*, *36*) (Figure 4B). Cell attachment to both hEF3A and *cyclo*-hEF3A was inhibited by heparin (Figure 4B). EDTA (5 mM) did not block on cell attachment to the hEF3A and *cyclo*-hEF3A peptides (Figure 4B), indicating that integrins are not involved in this cellular interaction. These results suggest that the hEF3A and *cyclo*-hEF3A peptides interact with membrane-associated heparin/heparan sulfate proteoglycans, such as syndecans.

Syndecan-4 Binding to hEF3A and cyclo-hEF3A. Because hEF3A and *cyclo*-hEF3A promoted heparin-dependent cell attachment (Figure 4), we examined syndecan binding to the peptides. The expression of syndecan-2 and -4 in the human dermal fibroblasts was previously determined by the reverse transcriptase polymerase chain reaction analysis (*11*). We focused on syndecan-4. Using a human fibroblast lysate in a solid phase assay, we found that hEF3A bound weakly to syndecan-4 (Figure 5A), while *cyclo*-hEF3A bound strongly in a dose-dependent manner (Figure 5A). The syndecan-4 binding to the peptides was significantly inhibited by heparin (Figure 5B). These results indicate that hEF3A and *cyclo*-hEF3A bind to syndecan-4 and that the conformation of *cyclo*-hEF3A is important for syndecan-4 binding. The *cyclo*-hEF3A peptide may be involved in syndecan-4-mediated cell attachment.

Neurite Outgrowth Activity of hEF3A and cyclo-hEF3A. The hEF3A and *cyclo*-hEF3A peptides were tested for neurite outgrowth activity using PC12 cells. As a negative control, hEF-1 peptide (*17*, *36*) was used. The hEF3A and *cyclo*-hEF3A promoted neurite outgrowth of PC12 cells in a dose-dependent manner (Figure 6A). The neurite outgrowth activity of *cyclo*-hEF3A was more potent than that of hEF3A (Figure 6A). The neurites of PC12 cells on *cyclo*-hEF3A were longer than that on hEF3A (Figure 6B). These results indicate that the conformation of the *cyclo*-hEF3A is important for neurite outgrowth activity.

Structural Analysis of cyclo-hEF3A. Next, we investigated the structure of *cyclo*-hEF3A using MD simulations (*28*−*34*). We determined the region corresponding to hEF3A in the laminin α2LG4 module, which has the crystal structure published (PDB ID: 1DYK), by sequence alignment (homologous_hEF3A; Figure 7A segment in red). The structure of homologous_hEF3A was used as the template for starting the simulations of peptides. For MD simulation, we prepared two peptides, 1DYK_SS and *cyclo*-hEF3A. 1DYK_SS has the same sequence as homologous_hEF3A except for the N and C termini, which are replaced by Cys residues with a disulfide bond between them. The simulation of 1DYK_SS was performed for measuring the effect of the disulfide bond on the conformation. The lowest-RMSD cluster of 1DYK_SS showed the average RMSD of 1.833 Å with the standard deviation of 0.342 Å and contained 27 structures. This result demonstrates that the conformation of residues 3−11 is not affected by the introduced disulfide bond. The lowest-RMSD cluster of *cyclo*-hEF3A showed the average RMSD of 2.023 Å with the standard deviation of 0.355 Å and contained 23 structures. The lowest-RMSD structure of 1DYK_SS is displayed (Figure 7B), for which the RMSD value is 0.906 Å. The lowest-RMSD structure of *cyclo*-hEF3A is displayed (Figure 7C), for which the RMSD value is 1.238 Å. The superimposition between the structures of the lowest-RMSD 1DYK_SS and *cyclo*-hEF3A is displayed (Figure 7D). The rmsd value between the two lowest-RMSD structures is 1.438 Å. These results indicate that the native state of *cyclo*-hEF3A is similar to that of 1DYK_SS. Taken together, the structure of *cyclo*-hEF3A is similar to that of the connecting E−F loop region in the human laminin α3LG4 module.

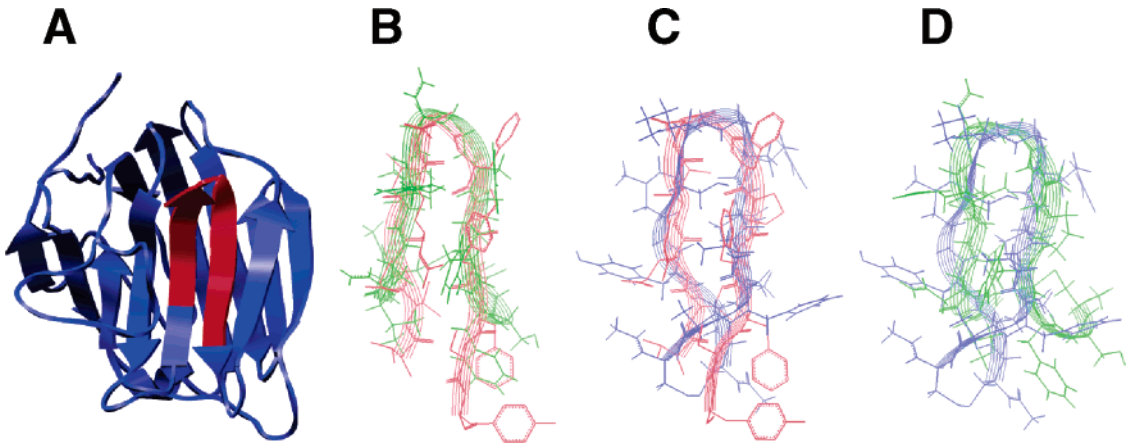

FIGURE 7: Structural analysis using MD simulation method. (A) Structure of homologous protein (laminin α2LG4 module). The segment in red is the region of homologous_hEF3A. (B) The segment in red is the structure of homologous_hEF3A, and the one in green is that of 1DYK_SS obtained from MD simulation. (C) The segment in red is the structure of homologous_hEF3A, and the one in blue is that of *cyclo*-hEF3A obtained from MD simulation. (D) The segment in green is the structure of 1DYK_SS obtained from MD simulation, and the one in blue is that of *cyclo*-hEF3A obtained from MD simulation. Two structures in each panel of B−D were superimposed for main chains (Cα, C, and N) of residues 3−11. The lowest-RMSD structure of 1DYK_SS or *cyclo*-hEF3A to the structure of homologous_hEF3A was selected for the display.

DISCUSSION

Cyclization of peptides restricts the conformation. Cyclic peptides might exhibit higher biological activity than their linear form due to reduction of the loss of entropy, which is required for the adaptation of linear peptides from its random coiled conformation to a frozen bound conformation. For example, RGD and YIGSR peptides, which were identified as cell-adhesive sequences, were cyclized and showed increased biological activity over their linear forms (*21*, *23*, *37*). The RGD and YIGSR peptides are located in loop regions of the fibronectin tenth type III module and the laminin β1 chain domain III, respectively (*19*, *20*). The loop structure of the peptides was important for the biological activity (*21*, *22*). Additionally, the cyclic peptides of the sequences may be useful for drug development and biomaterial research (*23*, *38*, *39*).

To obtain the enhanced biological activity by cyclization, a functional interaction of the three-dimensional structures of the cyclic peptide and receptor(s) is required. Inaccurate conformation of cyclic peptide leads to a reduction of binding affinity for its receptor(s) and causes a loss of the biological activity (*21*, *37*). Therefore, the peptide cyclization approach may be useful to investigate the structural requirements of a loop structure in a protein. Indeed, we previously demonstrated that the structural importance of connecting loop region between the E and the F strands on the LG4 module of laminin α1 and α4 chain using cyclic peptides (*17*, *18*). The cyc-EF-1Xm peptide (CLQLQEGRLHFXFDC, derived from mouse laminin α1 chain residues 2751−2763; "X" denotes the norleucine residue) increased cell attachment activity via α2β1 integrin (*17*). The *cyclo*-A4G82X (CTLFLAHGRLVFXC, derived from mouse laminin α4 chain residues 1514−1525) showed significantly enhanced syndecan-2-mediated cell attachment activity (*18*). These results suggest that the loop structure of the E−F loop region in the laiminin α1 and α4 LG4 modules is important for the biological activity.

In this report, we have demonstrated that *cyclo*-hEF3A had an enhanced inhibitory effect on heparin binding relative to the linear form. Using three different cell types, fibroblasts, HaCat cells, and PC12 cells, we showed that the *cyclo*-hEF3A peptide more strongly inhibited cell attachment to rec-α3LG4 than the linear peptide. We have also found that the *cyclo*-hEF3A peptide was more active for syndecan-4 binding than the linear form. Furthermore, we have carried out the MD simulations on the *cyclo*-hEF3A peptide and have demonstrated that the structure of *cyclo*-hEF3A is similar to that of the connecting E−F loop region in the parent molecule. These results suggest that the loop structure of the E−F connecting region of the human laminin α3LG4 module is important for syndecan-4-mediated cell attachment activity. We prepared three cyclic peptides, *cyclo*-hEF3A, *cyclo*-hEF3B, and *cyclo*-hEF3C, which contained KGR sequence. They showed different inhibitory effects on heparin binding and fibroblast attachment to rec-α3LG4. Although the peptides contain the KGR sequence, they could show different activity because of the conformation of the cyclic peptides is different according to the cyclized position. The *cyclo*-hEF3B and *cyclo*-hEF3C peptides showed the weaker activity than that of *cyclo*-hEF3A. Therefore, the conformation of *cyclo*-hEF3B and *cyclo*-hEF3C is supposed to be less similar to the loop structure of the E−F connecting region of the human laminin α3LG4 module.

Syndecans, cell surface heparan sulfate proteoglycans, are involved in laminin-mediated biological functions (*40*). We previously demonstrated that keratinocytes and fibroblasts bound to the rec-α3LG4 protein via syndecans and that rec-α3LG4 were colocalized with syndecans on the cell surface of dermal fibroblasts (*11*, *41*). Here, we have demonstrated that *cyclo*-hEF3A bound to syndecan-4 and promoted heparin-dependent fibroblast attachment and PC12 neurite outgrowth. Although *cyclo*-hEF3A showed stronger activity on syndecan-4 binding and PC12 neurite outgrowth than that of the linear peptide hEF3A, the cyclic peptide did not enhance the fibroblast attachment activity. Previously, syndecans were suggested to have unique functions other than cell attachment (*41*). Therefore, it is conceivable that the conformation of *cyclo*-hEF3A coated on plates did not allow effective interaction with fibroblasts. However, these mechanisms are not clear at that stage. Taken together, it is

suggested that the cell attachment and neurite outgrowth activities of *cyclo*-hEF3A are mediated by cell surface syndecans. Syndecans are expressed in basal keratinocytes at the wound edge of the skin (*42*) and also expressed in neural tissues (*43*−*46*). Syndecan-mediated cell signaling may be involved in wound repair (*41*, *47*) and nervous system development (*48*). Recently, the A3G756 peptide, which interacts with syndecans (*11*), has been found to promote wound healing in vivo, suggesting a potential therapeutic application (Momota et al., unpublished results). The *cyclo*-hEF3A peptide, which is a mimic of A3G756 and much smaller molecule as compared with A3G756, interacted with syndecans similar to A3G756. Therefore, the *cyclo*-hEF3A peptide has potential for therapeutic applications including wound healing and nerve regeneration.

In summary, we have investigated that the structural importance of the connecting E−F loop region of the human laminin α3 chain LG4 module using cyclic peptides. We have shown the *cyclo*-hEF3A peptide has more potent biological activities, including heparin binding, syndecan binding, cell attachment, and neurite outgrowth, when compared to the linear peptide. The *cyclo*-hEF3A peptide may be useful for the development of therapeutic reagents especially for wound healing and neuronal regeneration.

ACKNOWLEDGMENT

We are grateful to Dr. Hynda K. Kleinman (National Institute of Dental and Craniofacial Research, National Institutes of Health, Bethesda, MD) for critical reading of the manuscript.

REFERENCES

1. Sasaki, T., Fassler, R., and Hohenester, E. (2004) Laminin: The crux of basement membrane assembly, *J. Cell Biol. 164*, 959−963.
2. Colognato, H., and Yurchenco, P. D. (2000) Form and function: The laminin family of heterotrimers, *Dev. Dyn. 218*, 213−234.
3. Miner, J. H., Patton, B. L., Lentz, S. I., Gilbert, D. J., Snider, W. D., Jenkins, N. A., Copeland, N. G., and Sanes, J. R. (1997) The laminin alpha chains: expression, developmental transitions, and chromosomal locations of alpha1-5, identification of heterotrimeric laminins 8-11, and cloning of a novel alpha3 isoform, *J. Cell Biol. 137*, 685−701.
4. Iivanainen, A., Morita, T., and Tryggvason, K. (1999) Molecular cloning and tissue-specific expression of a novel murine laminin gamma3 chain, *J. Biol. Chem. 274*, 14107−14111.
5. Libby, R. T., Champliaud, M. F., Claudepierre, T., Xu, Y., Gibbons, E. P., Koch, M., Burgeson, R. E., Hunter, D. D., and Brunken, W. J. (2000) Laminin expression in adult and developing retinae: Evidence of two novel CNS laminins, *J. Neurosci. 20*, 6517−6528.
6. Rousselle, P., and Aumailley, M. (1994) Kalinin is more efficient than laminin in promoting adhesion of primary keratinocytes and some other epithelial cells and has a different requirement for integrin receptors, *J. Cell Biol. 125*, 205−214.
7. Aberdam, D., Aguzzi, A., Baudoin, C., Galliano, M. F., Ortonne, J. P., and Meneguzzi, G. (1994) Developmental expression of nicein adhesion protein (laminin-5) subunits suggests multiple morphogenic roles, *Cell Adhes. Commun. 2*, 115−129.
8. Smith, B. E., Bradshaw, A. D., Choi, E. S., Rouselle, P., Wayner, E. A., and Clegg, D. O. (1996) Human SY5Y neuroblastoma cell interactions with laminin isoforms: neurite outgrowth on laminin-5 is mediated by integrin alpha 3 beta 1, *Cell Adhes. Commun. 3*, 451−462.
9. Stipp, C. S., and Hemler, M. E. (2000) Transmembrane-4-superfamily proteins CD151 and CD81 associate with alpha 3 beta 1 integrin, and selectively contribute to alpha 3 beta 1-dependent neurite outgrowth. *J. Cell Sci. 113*, 1871−1882.
10. Culley, B., Murphy, J., Babaie, J., Nguyen, D., Pagel, A., Rousselle, P., and Clegg, D. O. (2001) Laminin-5 promotes neurite outgrowth from central and peripheral chick embryonic neurons, *Neurosci. Lett. 301*, 83−86.
11. Utani, A., Nomizu, M., Matsuura, H., Kato, K., Kobayashi, T., Takeda, U., Aota, S., Nielsen, P. K., and Shinkai, H. (2001) A unique sequence of the laminin α3 G domain binds to heparin and promotes cell adhesion through syndecan-2 and -4, *J. Biol. Chem. 276*, 28779−28788.
12. Kato, K., Utani, A., Suzuki, N., Mochizuki, M., Yamada, M., Nishi, N., Matsuura, H., Shinkai, H., and Nomizu, M. (2002) Identification of neurite outgrowth promoting sites on the laminin α3 chain G domain, *Biochemistry 41*, 10747−10753.
13. Momota, Y., Suzuki, N., Kasuya, Y., Kobayashi, T., Mizoguchi, M., Yokoyama, F., Nomizu, M., Shinkai, H., Iwasaki, T., and Utani, A. (2005) Laminin alpha3 LG4 module induces keratinocyte migration: Involvement of matrix metalloproteinase-9, *J. Recept. Signal Transduction Res. 25*, 1−17.
14. Hohenester, E., Tisi, D., Talts, J. F., and Timpl, R. (1999) The crystal structure of a laminin G-like module reveals the molecular basis of alpha-dystroglycan binding to laminins, perlecan, and agrin. *Mol. Cell 4*, 783−792.
15. Timpl, R., Tisi, D., Talts, J. F., Andac, Z., Sasaki, T., and Hohenester, E. (2000) Structure and function of laminin LG modules, *Matrix Biol. 19*, 309−317.
16. Okazaki, I., Suzuki, N., Nishi, N., Utani, A., Matsuura, H., Shinkai, H., Yamashita, H., Kitagawa, Y., and Nomizu, M. (2002) Identification of biologically active sequences in the laminin alpha 4 chain G domain, *J. Biol. Chem. 277*, 37070−37078.
17. Suzuki, N., Nakatsuka, H., Mochizuki, M., Nishi, N., Kadoya, Y., Utani, A., Oishi, S., Fujii, N., Kleinman, H. K., and Nomizu, M. (2003) Biological activities of homologous loop regions in the laminin alpha chain G domains, *J. Biol. Chem. 14*, 45697−45705.
18. Yokoyama, F., Suzuki, N., Haruki, M., Nishi, N., Oishi, S., Fujii, N., Utani, A., Kleinman, H. K., and Nomizu, M. (2004) Cyclic peptides from the loop region of the laminin alpha 4 chain LG4 module show enhanced biological activity over linear peptides, *Biochemistry 43*, 13590−13597.
19. Yamada, K. M. (1991) Adhesive recognition sequences, *J. Biol. Chem. 266*, 12809−12812.
20. Yamada, Y., and Kleinman, H. K. (1992) Functional domains of cell adhesion molecules, *Curr. Opin. Cell Biol. 4*, 819−823.
21. Aumailley, M., Gurrath, M., Muller, G., Calvete, J., Timpl, R., and Kessler, H. (1991) Arg-Gly-Asp constrained within cyclic pentapeptides. Strong and selective inhibitors of cell adhesion to vitronectin and laminin fragment P1, *FEBS Lett. 291*, 50−54.
22. Ostheimer, G. J., Starkey, J. R., Lambert, C. G., Helgerson, S. L., and Dratz, E. A. (1992) NMR constrained solution structures for laminin peptide 11. Analogs define structural requirements for inhibition of tumor cell invasion of basement membrane matrix, *J. Biol. Chem. 267*, 25120−25128.
23. Kleinman, H. K., Graf, J., Iwamoto, Y., Sasaki, M., Schasteen, C. S., Yamada, Y., Martin, G. R., and Robey, F. A. (1989) Identification of a second active site in laminin for promotion of cell adhesion and migration and inhibition of in vivo melanoma lung colonization, *Arch. Biochem. Biophys. 272*, 39−45.
24. Fujii, N., Oishi, S., Hiramatsu, K., Araki, T., Ueda, S., Tamamura, H., Otaka, A., Kusano, S., Terakubo, S., Nakashima, H., Broach, J. A., Trent, J. O., Wang, Z. X., and Peiper, S. C. (2003) Molecular-size reduction of a potent CXCR4-chemokine antagonist using orthogonal combination of conformation- and sequence-based libraries, *Angew. Chem., Int. Ed. Engl. 42*, 3251−3253.
25. Numa, F., Hirabayashi, K., Tsunaga, N., Kato, H., O'Rourke, K., Shao, H., Stechmann-Lebakken, C., Varani, J., Rapraeger, A., and Dixit, V. M. (1995) Elevated levels of syndecan-1 expression confer potent serum-dependent growth in human 293T cells, *Cancer Res. 55*, 4676−4680.
26. Greene, L. A., and Tischler, A. S. (1976) Establishment of a noradrenergic clonal line of rat adrenal pheochromocytoma cells which respond to nerve growth factor, *Proc. Natl. Acad. Sci. U.S.A. 73*, 2424−2428.
27. Nomizu, M., Kuratomi, Y., Malinda, M. K., Song, S.-Y., Miyoshi, K., Otaka, A., Powel, S. K., Hoffman, M. P., Kleinman, H. K., and Yamada, Y. (1998) Cell binding sequences in mouse laminin alpha1 chain, *J. Biol. Chem. 273*, 32491−32499.
28. Cornell, W. D., Cieplak, P., Bayly, C. I., Gould, I. R., Merz, K. M., Jr., Ferguson, D. M., Spellmeyer, D. C., Fox, T., Caldwell, J. W., and Kollman, P. A. (1995) A second generation force field

for the simulation of proteins, nucleic acids, and organic molecules, *J. Am. Chem. Soc. 117*, 5179−5197.
29. Onufriev, A., Bashford, D., and Case, D. A. (2000) Modification of the eneralized Born model suitable for macromolecules, *J. Phys. Chem. B 104*, 3712−3720.
30. Ryckaert, J. P., Ciccotti, G., and Berendsen, H. J. C. (1977) Numerical integration of the cartesian equations of motion of a system with constraints: Molecular dynamics of n-alkanes, *J. Comp. Phys. 23*, 327−341.
31. Terada, T., and Kidera, A. (2002) Generalized form of the conserved quantity in constant-temperature molecular dynamics, *J. Chem. Phys. 116*, 33−41.
32. Fukunishi, Y., Mikami, Y., and Nakamura, H. (2003) The filling potential method: A method for estimating the free energy surface for protein-ligand docking, *J. Phys. Chem. B 107*, 13201−13210.
33. Kim, J. G., Fukunishi, Y., Kidera, A., and Nakamura, H. (2003) Determination of multicanonical weight based on a stochastic model of sampling dynamics, *Phys. Rev. E 68*, 021110.
34. Kim, J. G., Fukunishi, Y., and Nakamura, H. (2004) Multicanonical molecular dynamics algorithm employing adaptive force-biased iteration scheme, *Phys. Rev. E 70*, 057103.
35. Nomizu, M., Kim, W. H., Yamamura, K., Utani, A., Song, S.-Y., Otaka, A., Roller, P. P., Kleinman, H. K., and Yamada, Y. (1995) Identification of cell binding sites in the laminin alpha 1 chain carboxyl-terminal globular domain by systematic screening of synthetic peptides, *J. Biol. Chem. 270*, 20583−20590.
36. Yokoyama, F., Suzuki, N., Kadoya, Y., Utani, A., Nakatsuka, H., Nishi, N., Haruki, M., Kleinman, H. K., and Nomizu, M. (2005) Bifunctional peptides derived from homologous loop regions in the laminin alpha chain LG4 modules interact with both alpha 2 beta 1 integrin and syndecan-2, *Biochemistry 44*, 9581−9589.
37. Pfaff, M., Tangemann, K., Muller, B., Gurrath, M., Muller, G., Kessler, H., Timpl, R., and Engel, J. (1994) Selective recognition of cyclic RGD peptides of NMR defined conformation by alpha IIb beta 3, alpha V beta 3, and alpha 5 beta 1 integrins, *J. Biol. Chem. 269*, 20233−20238.
38. Meyer, A., Auernheimer, J., Modlinger, A., and Kessler, H. (2006) Targeting RGD recognizing integrins: Drug development, biomaterial research, tumor imaging and targeting, *Curr. Pharm. Des. 12*, 2723−2747.
39. Oishi, S., Kamano, T., Niida, A., Odagaki, Y., Hamanaka, N., Yamamoto, M., Ajito, K., Tamamura, H., Otaka, A., and Fujii, N. (2002) Diastereoselective synthesis of new psi[(E)-CH═CMe]- and psi[(Z)-CH═CMe]-type alkene dipeptide isosteres by organocopper reagents and application to conformationally restricted cyclic RGD peptidomimetics, *J. Org. Chem. 67*, 6162−6173.
40. Delehedde, M., Lyon, M., Sergeant, N., Rahmoune, H., and Fernig, D. G. (2001) Proteoglycans: Pericellular and cell surface multireceptors that integrate external stimuli in the mammary gland, *J. Mammary Gland Biol. Neoplasia 6*, 253−273.
41. Utani, A., Momota, Y., Endo, H., Kasuya, Y., Beck, K., Suzuki, N., Nomizu, M., and Shinkai, H. (2003) Laminin alpha 3 LG4 module induces matrix metalloproteinase-1 through mitogen-activated protein kinase signaling, *J. Biol. Chem. 278*, 34483−34490.
42. Gallo, R., Kim, C., Kokenyesi, R., Adzick, N. S., and Bernfield, M. (1996) Syndecans-1 and -4 are induced during wound repair of neonatal but not fetal skin, *J. Invest. Dermatol. 107*, 676−683.
43. Ethell, I. M., and Yamaguchi, Y. (1999) Cell surface heparan sulfate proteoglycan syndecan-2 induces the maturation of dendritic spines in rat hippocampal neurons, *J. Cell Biol. 144*, 575−586.
44. Teel, A. L., and Yost, H. J. (1996) Embryonic expression patterns of Xenopus syndecans, *Mech. Dev. 59*, 115−127.
45. Inatani, M., Haruta, M., Honjo, M., Oohira, A., Kido, N., Takahashi, M., Honda, Y., and Tanihara, H. (2001) Upregulated expression of N-syndecan, a transmembrane heparan sulfate proteoglycan, in differentiated neural stem cells, *Brain Res. 920*, 217−221.
46. Inatani, M., Honjo, M., Oohira, A., Kido, N., Otori, Y., Tano, Y., Honda, Y., and Tanihara, H. (2002) Spatiotemporal expression patterns of N-syndecan, a transmembrane heparan sulfate proteoglycan, in developing retina, Invest, *Ophthalmol. Vis. Sci. 43*, 1616−1621.
47. Midwood, K. S., Valenick, L. V., Hsia, H. C., and Schwarzbauer, J. E. (2004) Coregulation of fibronectin signaling and matrix contraction by tenascin-C and syndecan-4, *Mol. Biol. Cell. 15*, 5670−5677.
48. Rhiner, C., Gysi, S., Frohli, E., Hengartner, M. O., and Hajnal, A. (2005) Syndecan regulates cell migration and axon guidance in *C. elegans*, *Development 132*, 4621−4633.
49. Ryan, M. C., Tizard, R., VanDevanter, D. R., and Carter, W. G. (1994) Cloning of the LamA3 gene encoding the alpha 3 chain of the adhesive ligand epiligrin. Expression in wound repair, *J. Biol. Chem. 269*, 22779−22787.

BI062098L